

# Color Equivariant Network

Felix O’Mahony  
University of Oxford  
Oxford, UK  
felixomahony@gmail.com

Yulong Yang  
Princeton University  
Princeton, NJ, USA  
yulong.yang@princeton.edu

Christine Allen-Blanchette  
Princeton University  
Princeton, NJ, USA  
ca15@princeton.edu

## Abstract

*Group equivariant convolutional neural networks have been designed for a variety of geometric transformations from 2D and 3D rotation groups, to semi-groups such as scale. Despite the improved interpretability, accuracy and generalizability afforded by these architectures, group equivariant networks have seen limited application in the context of perceptual quantities such as hue and saturation, even though their variation can lead to significant reductions in classification performance. In this paper, we introduce convolutional neural networks equivariant to variations in hue and saturation by design. To achieve this, we leverage the observation that hue and saturation transformations can be identified with the 2D rotation and 1D translation groups respectively. Our hue-, saturation-, and fully color-equivariant networks achieve equivariance to these perceptual transformations without an increase in network parameters. We demonstrate the utility of our networks on synthetic and real world datasets where color and lighting variations are commonplace.*

## 1. Introduction

The tremendous progress of image classification in the last decade can be readily attributed to the development of deep convolutional neural networks [19, 24, 30]. The highly non-linear mapping and large parameter space does not lend itself to interpretation easily, but even in early networks, representations of geometry and color were observed and recognized for their importance in representation learning [24, 26]. While a relatively large body of literature has worked to improve the robustness of convolutional neural networks to geometric transformations [4, 7, 16, 17, 20, 28], improving their robustness to perceptual variation has garnered considerably less attention.

A commonly used heuristic for improving network robustness to color variation is to perform mean subtraction and normalization on training set examples. This approach can work well when the training and testing datasets are

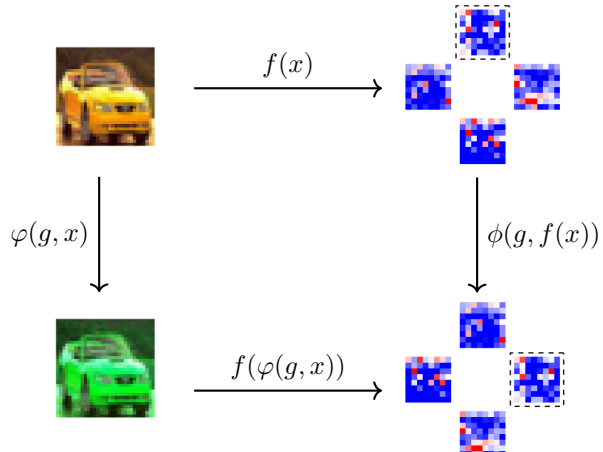


Figure 1. Hue equivariance. The equivariance of our hue equivariant model is illustrated by the commutativity of the (hue) rotation and neural network mapping. A hue rotation of  $90^\circ$  in the input image space (top-left to bottom-left), results in a feature map rotation at each layer of the network (top-right to bottom-right).

drawn from the same distribution; however, for data that are collected at different points in time, or with different sensors, this is not likely to be the case. Consider, for example, the case of medical imaging where images of tissue samples collected from different labs (or from the same lab at different points in time) may have different characteristics due to variability in data collection protocols or imaging processes [33]. This variability presents a significant challenge for convolutional neural networks which have been found to be sensitive to color variations even on the level of individual blocks [11]. Moreover, when presented with color perturbations, conventional networks exhibit a significant drop in classification performance [10]. One approach to mitigate the effect of color variation is to ignore color entirely by enforcing color invariance. This can be done by converting input images to grayscale, or enforcing representation

similarity across color as is done in [27]. This approach has its own challenges, however, since in many domains, color is an important cue for classification. Another approach is to use dataset augmentation, a technique that can improve robustness in the presence of known transformations [3]. This approach, however, requires extended training times and is not likely to offer improved interpretability.

In this work, we address the challenge of neural network sensitivity to color variation by leveraging the geometric structure of color in a group equivariant network. Geometric deep learning has gained strong interest in recent years due to its ability to capture information in interpretable and generalizable representations; by using a group equivariant architecture, we inherit these characteristics for the context of color variation. Using this approach, our network retains color information in a structured representation throughout the processing pipeline, thus allowing color information to be used and/or discarded with intentionality.

We represent color in the hue saturation luminance color space, and leverage the insight that the hue, and saturation can be modeled with geometric group structure. Specifically, we identify variations in hue with the 2D rotation group, and variations in saturation with the 1D translation group. With this identification, we propose a group equivariant network where variations in hue and saturation are represented as a geometric transformations.

To summarize, our key contributions are:

- We introduce networks that are equivariant to shifts in hue and saturation, without requiring an increase in the number of network parameters.
- Our networks perform on par or better than conventional architectures in the presence of unseen color combinations on synthetic, and real world datasets.
- Our networks produce interpretable feature representations that are useful for downstream tasks such as color based sorting.

## 2. Related work

**Group Equivariant Networks** The strong generalization performance of convolutional neural networks on image processing tasks is attributed, in part, to the equivariance of planar convolution to 2D translations. This insight has garnered considerable attention and led to a strong interest in the development of convolutional neural networks equivariant to other symmetry groups [9, 22]. Previous works introduce group equivariant convolutional networks for finite and continuous groups. A framework for finite group convolution was developed in [7], and demonstrated for the 2D rotation, and reflection groups. The authors achieve equivariance to specific symmetry groups by convolving input images and feature maps with the group orbit of a learned filter bank. In [36], the authors design for equivariance to the continuous 2D rotation group by constraining filter rep-

resentations to have circular harmonic structure.

Group equivariant networks have also been designed for use in the context of scale symmetry. In [12], the authors represent input images in log-polar coordinates where 2D rotation and scale transformations present as 2D translations. To navigate the semi-group structure of scale transformations, the authors in [35] approximate the scale space as finite and use dilated convolutions in a group equivariant architecture. The SREN network proposed in [31] designs for equivariance to the continuous 2D rotation and isotropic scaling group by constraining filter representations to be expressed as the linear combination of a windowed Fourier basis.

Group equivariant networks have also been designed for groups acting in higher dimensions. For 3D rotational symmetry, [32] and [13] use a spherical harmonics based representation with 3D point clouds and spherical image inputs respectively; and [2] introduce an equivariant network for transformations of the Euclidean group in 3D. In [14], the authors introduce a framework for general Lie groups whose exponential map is surjective, and [8] introduces a framework for more general manifolds. By designing for known symmetries in the task, these works provide improved interpretability, training efficiency and generalizability over conventional convolutional networks.

Other works encourage transformation equivariance using a soft penalty term on representation dissimilarity [18, 26]. These methods are separate from the group equivariant network literature, and different from what we propose. Our model leverages the geometric structure of hue and saturation to design a hue-saturation equivariant network bringing the benefits of group equivariant networks to perceptual transformations.

**Color Invariance** Several prior works attempt to mitigate the effect of color variation in image processing tasks, for example, in [6], the authors represent images in a color space where pixel values are invariant to changes in luminance for luminance invariant image segmentation, and in [27], the authors penalize changes in their latent representations due to color variation for color invariant skin lesion identification. While color invariance resolves the effect of color variation, color has been identified as an important cue in neural network representation learning [10, 11] which is discordant with the goal of color invariance. In contrast to these approaches, our work leverages the geometric structure of hue, and saturation to construct a convolutional neural network equivariant to variations in these quantities by design.

Most similar to ours is the model proposed in [29], a hue equivariant network for improved network performance in the presence of color variation. Our color equivariant networks differ from the work proposed in [29] in three im-

portant ways. First, our networks are fully equivariant, in contrast to the hybrid networks proposed in [29]. Second, we lift the input image instead of the filters of the first layer which circumvents the issue of invalid hue rotations suffered by the network in [29]. Finally, we introduce networks equivariant to hue and saturation, which together provide full color equivariance and is unique to our approach.

### 3. Preliminaries

In this section we describe our notation, and review definitions of the group action, equivariance, and group convolution.

**Notation.** We use  $f^l$  to denote the  $l$ -th feature map ( $f^0$  to denote an input image), and  $f_j^l$  to denote the  $j$ -th channel of that feature map. We use  $\psi_i^l$  to denote the  $i$ -th filter of the  $l$ -th layer, and  $\psi_{i,j}^l$  to denote the  $j$ -th channel of that filter.

**Group action.** Adapted from [15]. Given a set  $X$  and a group  $G$ , the action of the group  $G$  on  $X$  is a function  $\varphi : G \times X \rightarrow X$  satisfying the following:

1. For all  $g, h \in G$  and all  $x \in X$

$$\varphi(g, \varphi(h, x)) = \varphi(gh, x) \quad (1)$$

2. For all  $x \in X$

$$\varphi(1, x) = x \quad (2)$$

where  $1 \in G$  is the identity element of  $G$ .

The set  $X$  is called a (left)  $G$ -set.

**Equivariance.** Adapted from [15]. Given two  $G$ -sets  $X$  and  $Y$ , and group actions  $\varphi : G \times X \rightarrow X$  and  $\phi : G \times Y \rightarrow Y$ , a function  $f : X \rightarrow Y$  is said to be equivariant, if and only if for all  $x \in X$ , and  $g \in G$ ,

$$f(\varphi(g, x)) = \phi(g, f(x)). \quad (3)$$

When  $f$  is invariant to the action of  $G$ , the group action  $\phi$  is the identity map and we write

$$f(\varphi(g, x)) = f(x). \quad (4)$$

The equivariance of our network to hue shifts is illustrated in Figure 1.

**Group convolution.** In a conventional CNN, the input to convolution layer  $l$ , denoted  $f^l : \mathbb{Z}^2 \rightarrow \mathbb{R}^{K^l}$ , is convolved with a set of  $K^{l+1}$  filters, denoted  $\psi_i^l : \mathbb{Z}^2 \rightarrow \mathbb{R}^{K^l}$ , where  $i$  ranges from 1 to  $K^{l+1}$ . The result of the convolution can be written:

$$f_i^{l+1} = [f^l * \psi_i^l](x) = \sum_{y \in \mathbb{Z}^2} \sum_{k=1}^{K^l} f_k^l(y) \psi_{i,k}^l(x - y), \quad x \in \mathbb{Z}^2. \quad (5)$$

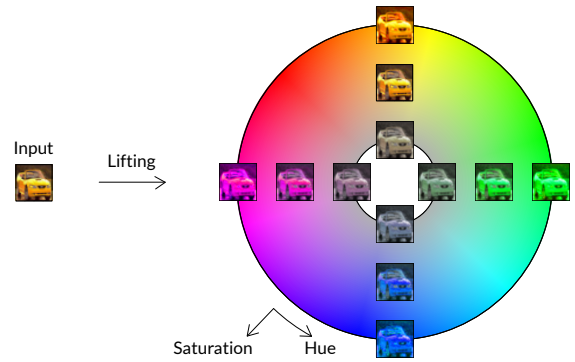


Figure 2. Lifting layer. An input image (left) is “lifted” to the hue-saturation group (right) by shifting its hue and saturation values.

The convolution of conventional CNNs is equivariant to the action of the group  $(\mathbb{Z}^2, +)$ , that is, the group formed by summing over the integers. The more general group convolution can be written:

$$[f^l * \psi_i^l](g) = \sum_{h \in G} \sum_{k=1}^{K^l} f_k^l(h) \psi_{i,k}^l(h^{-1}g), \quad (6)$$

and is equivariant to the action of the group  $G$ .

### 4. Method

In this section we present our color equivariant network. We begin by presenting definitions for the hue and saturation groups and their group actions, then define the lifting layers, and group convolution layers for our color equivariant networks.

**Hue group and group action.** In the HSL color space, hue is represented by angular position, and can therefore be identified with the 2D rotation group. As in group equivariant network [7], we consider a finite group representation. Specifically, we identify elements of the discretized hue group,  $H_N$ , with those of the cyclic group  $C_N$ .

We define the action of hue group on HSL images,  $x \in X$  where  $x : \mathbb{Z}^2 \rightarrow \mathbb{R}^3$ , and functions on the discrete hue group,  $y \in Y$ , where  $y : \mathbb{Z}^2 \times H_N \rightarrow \mathbb{R}^K$ . An element of the hue group acts on an HSL image by the group action  $\varphi_h : H_N \times X \rightarrow X$ , which shifts the hue channel of the image. Concretely, for an HSL image  $x \in X$  defined as the concatenation of hue, saturation and luminance channels, i.e.,  $x = (x_h, x_s, x_l)$ , the action of an element  $h_i$  of the hue group  $H_N$  is given by

$$\varphi_h(h_i, x) = ((x_h + h_i) \bmod 255, x_s, x_l), \quad (7)$$

where  $(\cdot) \bmod (\cdot)$  denotes the modulus operation and is applied to the pixel value rather than its corresponding degree.

An element of the hue group acts on a function on the discrete hue group by the group action  $\phi_h : H_N \times Y \rightarrow Y$ , which “rotates” the function on the group. Concretely, for a function  $f$  on the discrete hue group  $H_N$  defined as the concatenation of functions  $f = (f_1, \dots, f_N)$ , the action of an element  $h_i$  in the hue group  $H_N$  is given by

$$\phi_h(h_i, f) = (f_{(1+i)(\bmod N)}, \dots, f_{(N+i)(\bmod N)}). \quad (8)$$

**Saturation group and group action.** In the HSL color space, saturation can be represented by a real number in the interval  $[0, 1]$ . We introduce two approximations to give group structure to the saturation space. First, we observe that there is a bijection between the real numbers and the open interval  $(0, 1)$ , so we use the structure of the group  $(\mathbb{R}, +)$ . Second, we consider a finite subset of the group, a necessary and commonly used practice in both conventional CNNs (recall that the translation group is infinite) and group-equivariant CNNs such as [35].

We define the action of the saturation group on HSL images,  $x \in X$  where  $x : \mathbb{Z}^2 \rightarrow \mathbb{R}^3$ , and functions on the discrete saturation group,  $y \in Y$ , where  $y : \mathbb{Z}^2 \times S_N \rightarrow \mathbb{R}^K$ . An element of the saturation group acts on an HSL image by the group action  $\varphi_s : S_N \times X \rightarrow X$ , which shifts the saturation channel of the image. Concretely, for an HSL image  $x \in X$  defined as the concatenation of hue, saturation and luminance channels, i.e.,  $x = (x_h, x_s, x_l)$ , the action of an element  $s_i$  of the saturation group  $S_N$  is given by

$$\varphi_s(s_i, x) = (x_h, \min(x_s + s_i, 255), x_l). \quad (9)$$

An element of the saturation group acts on a function on the discrete saturation group by the group action  $\phi_s : S_N \times Y \rightarrow Y$ , which “translates” the function on the group. Concretely, for a function  $f$  on the discrete saturation group  $S_N$  defined as the concatenation of functions  $f = (f_1, \dots, f_N)$ , the action of an element  $s_i$  in the saturation group  $S_N$  is given by

$$\phi_s(s_i, f) = (f_{1+i}, \dots, f_N, \underbrace{\mathbf{0}, \dots, \mathbf{0}}_i). \quad (10)$$

**Hue-Saturation group action.** We define the action of the hue-saturation group as a composition of the hue and saturation group actions. An element of the hue-saturation group acts on an HSL image by the group action  $\varphi_{hs} : H_N \times S_M \times X \rightarrow X$ , which shifts both the hue and saturation channels of the image. For an HSL image  $x \in X$  defined as the concatenation of hue, saturation and luminance channels, i.e.,  $x = (x_h, x_s, x_l)$ , the action of an element  $(h_i, s_j)$  of the hue-saturation group  $H_N \times S_M$  is given by

$$\varphi_{hs}((h_i, s_j), x) = \varphi_h(h_i, \varphi_s(s_j, x)). \quad (11)$$

An element of the hue-saturation group acts on a function on the discrete saturation group by the group action  $\phi_{hs} : H_N \times S_M \times Y \rightarrow Y$ , which “rotates” and “translates” the function on the group. Concretely, for a function  $f$  on the discrete hue-saturation group  $H_N \times S_M$  defined as the concatenation of functions  $f = (f_{11}, \dots, f_{1M}, f_{21}, \dots, f_{NM})$ , the action of an element  $(h_i, s_j)$  in the hue-saturation group  $H_N \times S_M$  is given by

$$\phi_{hs}((h_i, s_j), f) = \phi_h(h_i, \phi_s(s_j, f)). \quad (12)$$

**Lifting layer.** The first layer of a group convolutional neural network “lifts” the input image to the group (see Figure 2). We can lift an input image to the product space of the image grid  $\mathbb{Z}^2$ , and discretized hue shifts  $H_N = \{h_0, h_1, \dots, h_N\}$ , by convolving with hue shifted filters,

$$[f^0 * \psi_i^0](g_{x,j}) = \sum_{y \in \mathbb{Z}^2} \sum_{k=1}^{K^0} f_k^0(y) h_j \psi_{i,k}^0(x - y). \quad (13)$$

Here we denote an element of the product space  $g_{x,i}$ , where the subscript  $x$  references an element of  $\mathbb{Z}^2$ , and  $j$  references the element  $h_j$  in  $H_N$ . The input image  $f^0$  and lifting filters  $\psi_{m,n}$  are functions on  $\mathbb{Z}^2$ .

Lifting to the group can also be achieved by transforming the input image rather than the filters,

$$f^1(g_{x,j}) = \varphi_h(h_j, f^0)(x). \quad (14)$$

We use this alternative in our implementation as it is both simple and does not result in pixels falling outside the RGB cube as in [29]. The lifting layers for the saturation group, and hue-saturation group are constructed analogously.

**Equivariance of the lifting layer.** We can show that our lifting layer is equivariant to hue shifts. We let  $f^1(g_{x,j}) = \varphi_h(h_j, f^0)(x)$  as in equation 14 and show that a hue shift of  $f^0$  results in a hue shift of  $f^1$ . In the first step we use the fact that  $\varphi_h$  is a group action (see Appendix C.1), and in the second step we use commutativity of the hue group:

$$\varphi_h(h_j, \varphi_h(h_m, f^0))(x) = \varphi(h_j h_m, f^0)(x) \quad (15)$$

$$= \varphi_h(h_m h_j, f^0)(x) \quad (16)$$

$$= \varphi_h(h_m, \varphi_h(h_j, f^0))(x) \quad (17)$$

$$= \varphi_h(h_m, f^1(g_{x,j})). \quad (18)$$

Equivariance of the saturation, and hue-saturation lifting layers can be shown analogously.

**Group convolution layer.** For all layers after the first layer, the feature maps  $f^l$  are on the product space  $\mathbb{Z}^2 \times H_N$ . Since hue shifts can only be performed on three dimensional inputs, we leverage the identification of hue shifts

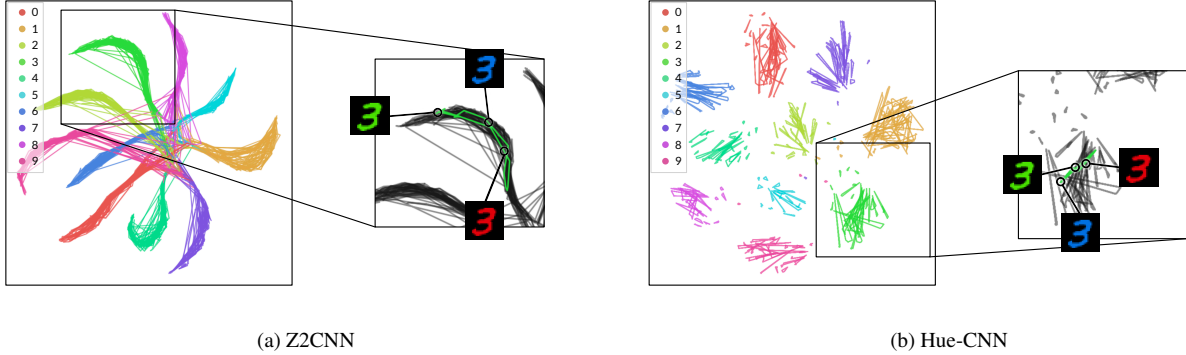


Figure 3. Hue shift MNIST feature map visualization. We compare the feature map trajectories of MNIST digits as their hue is varied from 1 to 360°. The color of the trajectory corresponds to the class label. (a) tSNE projection of hue shifted feature map trajectories in the Z2CNN baseline model. As the hue of the input changes, the location of the digit in the feature space changes significantly. (b) tSNE projection of hue shifted feature map trajectories in our hue-equivariant CNN. In contrast to the Z2CNN baseline, the location of the digit in the feature space changes minimally.

	A/A	A/B	Params
Z2CNN	<b>1.54 (0.10)</b>	57.38 (22.06)	22,130
Hue-4*	1.97 (0.25)	2.08 (0.15)	25,690
Hue-3*	1.79 (0.25)	<b>1.81 (0.28)</b>	22,658
CEConv	1.79 (0.13)	1.83 (0.19)	28,739
CEConv-2	2.81 (0.44)	5.08 (0.18)	30,539

Table 1. Classification error on the hue shift MNIST dataset. Our networks are marked with (\*). The number of parameters for all networks is reported.

with the discrete 2D rotation group, i.e.,  $H_N \cong C_N$  and interpret the feature maps  $f^l$  as functions on the product space  $G := \mathbb{Z}^2 \times C_N$ . With this interpretation we perform group convolution on  $G$  as follows,

$$[f^l * \psi_i^l](g) = \sum_{h \in H} \sum_{k=1}^{K^0} f_k^l(h) \psi_{i,k}^l(g^{-1}h), \quad (19)$$

where  $\psi^l$  is a function on  $G$ . Group convolution on the saturation, and hue-saturation groups are performed analogously.

## 5. Experiments

In this section we demonstrate the strength of our method in the presence of global and local hue variation, and global saturation variation on synthetic and real world datasets. We also demonstrate the ability of our model to perform color dependent tasks such as sorting.

### 5.1. Hue-shift MNIST: Global hue equivariance

We evaluate the performance of our models in the presence of global hue shifts on a classification dataset derived from

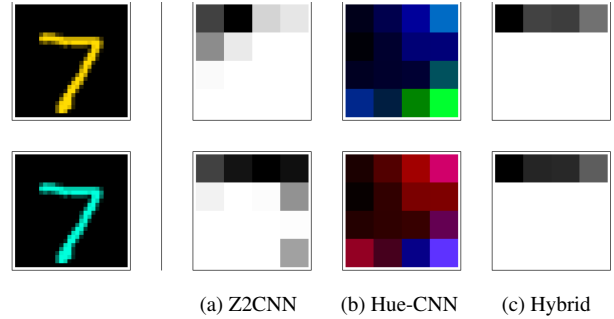


Figure 4. Comparison of feature maps for equivariant and non-equivariant architectures. In the conventional network (a), the relationship between feature maps is unclear. In our model (b), a hue shift in the input results in a predictable hue shift of the internal representations. In the hybrid network (c), the feature maps appear approximately invariant to hue shift.

MNIST [25]. The dataset consists of 70k examples, 60k of which are used for training and 10k of which are used for testing.

To test the performance of our models, we partition the testing dataset into two subsets: an in-distribution testing set and an out-of-distribution testing set. In the training set and in-distribution testing set, denoted subset  $A$ , digits are colored with a randomly selected hue between 0° and 240° (see Figure 6a). In the out-of-distribution testing set, subset  $B$ , digits are colored with a randomly selected hue between 240° and 360° (see Figure 6b).

Model performance is reported in Table 1. On the in-distribution test case ( $A/A$ ), the performance of our hue-equivariant models (Hue-x) and the conventional model (Z2CNN) are comparable. On the out-of-distribution test case ( $A/B$ ), the performance of our hue-equivariant models is preserved, while the performance of the conventional

Network	Group	<i>A/A</i>	<i>A/B</i>	<i>A/C</i>	Params
ResNet18	$\mathbb{Z}^2$	0.00 (0.00)	38.53 (3.19)	17.73 (0.90)	11.17M
	Hue-4*	<b>0.00</b>	<b>0.00</b>	<b>0.00</b>	11.17M
ResNet44	$\mathbb{Z}^2$	0.00 (0.00)	41.34 (1.73)	22.29 (10.80)	2.64M
	Hue-4*	<b>0.00 (0.00)</b>	<b>0.00 (0.00)</b>	<b>0.00 (0.00)</b>	2.63M
CNN	$\mathbb{Z}^2$	0.00 (0.00)	51.25 (9.59)	26.66 (19.60)	20,192
	Hue-4*	<b>0.00 (0.00)</b>	<b>0.00 (0.00)</b>	<b>0.00 (0.00)</b>	21,832
	Hue-3*	0.00 (0.00)	0.03 (0.04)	0.04 (0.03)	19,478
CEConv		0.00 (0.00)	0.02 (0.03)	0.05 (0.04)	26,441

Table 2. Classification error on the 3D Shapes dataset. Our networks are marked with (\*). The number of parameters for all networks is reported.

model deteriorates significantly.

The performance gap on the out-of-distribution test case can be attributed to the difference in internal representation structure. To understand this better, we generate feature representation trajectories in the penultimate layer of our network and the baseline architecture. Feature representation trajectories are generated by continuously varying the hue of an input image, and visualized using tSNE projection (see Figure 3). For the baseline architecture, the trajectories of different digits overlap for some hues (Figure 3a). For our model, the trajectories of different digits are confined to separate clusters (Figure 3b).

We also compare our model to the hue-equivariant (CEConv), and hybrid network (CEConv-2) proposed in [29]. With the same hue discretization (i.e.,  $N = 3$ ), our model performs comparably with the baseline hue-equivariant model, and out performs the baseline hybrid model. We investigate differences in the internal representations of our model, the conventional architecture, and the baseline hybrid model in Figure 4. For each network, we visualize the feature maps generated for a hue rotated input. For a hue discretization of  $N = 3$ , the network feature maps have three channels and can be visualized as an RGB image. Only the feature maps of our network shift predictably in response to hue shifts of the input.

## 5.2. Hue-shift 3D Shapes: Local hue equivariance

We evaluate the performance of our models in the presence of local hue shifts on the 3D Shapes classification dataset [5]. The dataset consists of RGB images of 3D shapes; the color of the shape, the floor, and the walls vary across examples, as do the scale and orientation of the shape.

To test the performance of our models, we partition the dataset into four subsets: a training set of 48k examples, and a test set of 12k examples. In-distribution and out-of-distribution test sets differ by color range assigned to the shape, floor and walls. In the training set and in-distribution testing set (subset *A*), the color of the wall, the floor and the shape are randomly selected from the first half of the color

space (colors 0-4 as defined in [5]). The out-of-distribution testing sets are designed to measure robustness to global hue shift, and local hue shift. In the out-of-distribution testing set designed to measure robustness to global hue shift (subset *B*), the color of the wall, the floor and the shape are randomly selected from the second half of the color space (colors 5-9 as defined in [5]). In the out-of-distribution testing set designed to measure robustness to local hue shift (subset *C*), the color of the wall and the floor are randomly selected from the first half of the color space, and the color of the shape is randomly selected from the second half of the color space.

Model performance is reported in Table 2. Our hue-equivariant architectures outperform all baseline models for all test cases. Noteably, our hue-equivariant architecture with CNN backbone and  $\sim 22k$  parameters outperforms both the ResNet44 and ResNet18 architectures with  $\sim 2M$  and  $\sim 11M$  parameters respectively.

## 5.3. Camelyon17: Saturation shift in the wild

We evaluate the performance of our model in the presence of natural saturation shifts on the Camelyon17 classification dataset [1]. The dataset consist of images of human tissue collected from five different hospitals. Variation in tissue images results from variation in the data collection and processing procedures. The dataset consists of 387,490 examples, 302,436 of which are used for training and 85,054 of

	Error	Params
ResNet50	28.91 (7.58)	23.5M
Sat- $d_1$ *	19.60 (2.08)	23.3M
Sat- $d_2$ *	<b>16.08 (2.68)</b>	23.3M
Sat- $d_3$ *	24.53 (7.13)	23.3M
Sat- $d_4$ *	23.57 (6.04)	23.3M

Table 3. Classification error on the Camelyon17 dataset. Our networks are marked with (\*). The number of parameters for all networks is reported.

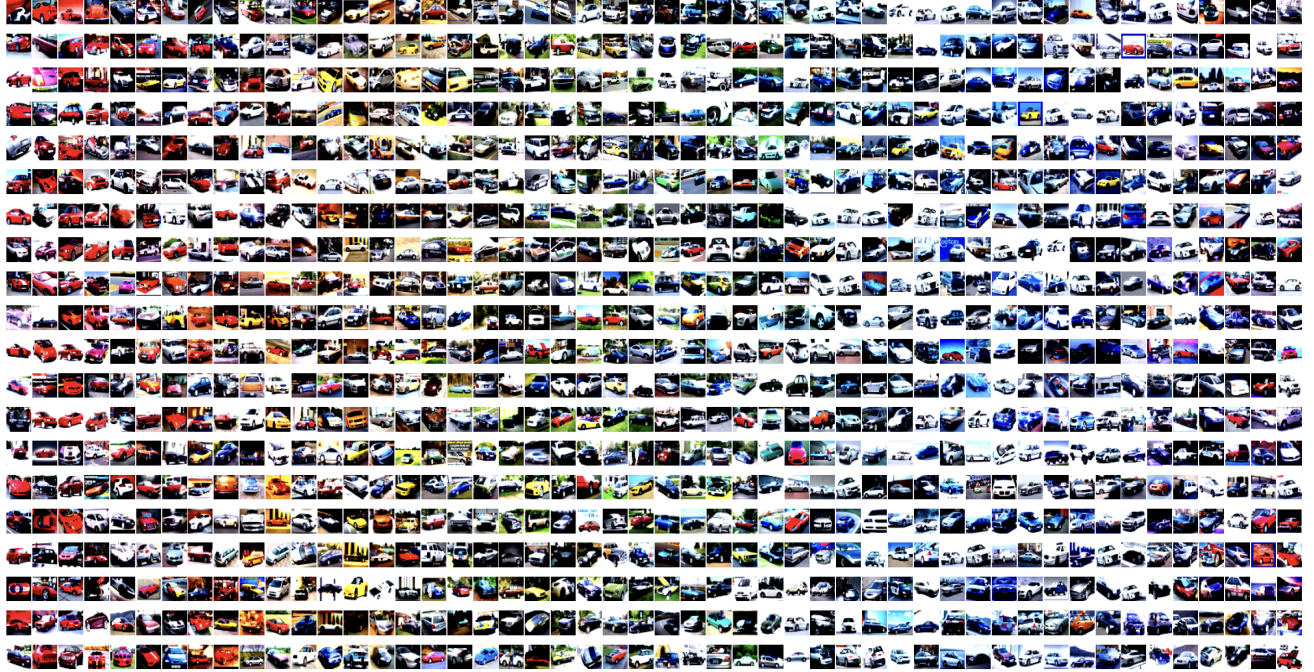


Figure 5. CIFAR-10 automobile class sorted by hue.

which are used for testing. Hospitals 1, 2, and 3 are represented in the training set, hospital 5 is represented in the testing set.

We present experimental results for four discretizations of the saturation space. Our choice of discretizations, i.e.,  $d \in \{1/20, 1/10, 3/20, 1/2\}$ , are determined with consideration of the saturation range of the training set. For a given choice of discretization  $d$ , an element  $s_i \in S_N$  shifts the saturation of an input image by  $s_i = i * d * 255$ . We limit computational expense of lifting and convolution by performing these operations over the truncated set  $\{s_{-1}, s_0, s_1\}$ . Model performance is reported in Table 3. The performance of our saturation-equivariant models out perform all other models, and the performance of our hue-equivariant model is on par with the baseline model.

#### 5.4. CIFAR-10: Color shift in the wild

We evaluate the performance of our model in the presence of natural hue shifts on the CIFAR-10 [23] classification dataset. The dataset consists of 60k examples, 40k of which are used for training, 10k for validation, and 10k for testing. Model performance is reported in Table 4. The performance of our color-equivariant models are comparable to the baseline model.

While our hue-equivariant model performs on par with the baseline model, the structure of the representation can be leveraged for tasks that are not possible with the baseline alone. To illustrate this, we use our model to sort images in the automobile class by hue (see Figure 5). To produce

	Error	Params
ResNet44	<b>7.86 (1.14)</b>	2.64M
Hue-4*	8.83 (0.64)	2.63M
Sat- $d_1$ *	10.45 (1.76)	2.55M
Sat- $d_2$ *	10.26 (0.43)	2.55M
Sat- $d_3$ *	9.24 (0.27)	2.55M
Hue-Sat- $d_1$ *	10.68 (0.78)	2.50M
Hue-Sat- $d_2$ *	11.13 (0.84)	2.50M
Hue-Sat- $d_3$ *	11.16 (0.38)	2.50M
Hue-3*	8.42 (0.39)	2.55M
CEConv	8.86 (0.33)	1.15M

Table 4. Classification error on the CIFAR-10 dataset. Our networks are marked with (\*). The number of parameters for all networks is reported.

an hue ordering, we compute the hue shifted pairwise Euclidean distance between the penultimate layer hue group feature maps of instances in the automobile class. Images  $x_1$  and  $x_2$  are close in the hue space if

$$d(\Phi(x_1), \Phi(x_2)) = \min_i d(h_i \Phi(x_1), \Phi(x_2)), \quad (20)$$

where  $\Phi(x_i)$  denotes the penultimate layer hue group feature map for image  $i$ .

## 6. Conclusion

In this paper we address the challenge of learning hue- and saturation-equivariant representations. Leveraging the ob-

servation that these perceptual transformations have geometric structure, we propose a group structure for each, and a group convolutional neural network that is equivariant to the transformations by design. By encoding perceptual variation in a finite group structure, we can use learned representations for color based sorting. Moreover, with an efficient implementation, our network achieves comparable performance to conventional architectures with comparable parameters.

## 6.1. Limitations and future work

While our method is equivariant to hue and saturation by design, it is not guaranteed to be equivariant to luminance. However, since luminance is computed as a linear combination of the red, green and blue channel values of an input image, if the preprocessing statistics (e.g., data mean) on the training set are valid for the testing set, luminance is approximately unchanged.

Additional limitations derive from our choice of equivariant modeling structure. Group equivariant networks are more computationally expensive than their conventional counterparts since they require computation of the filter orbit at each layer. This is compounded with the requirement for a finite filter orbit which can at best approximate a continuous group. Future work will investigate a Fourier series representation of the group to resolve both of the aforementioned challenges.

## 7. Acknowledgements

We would like to thank members of the CAB Lab for valuable discussions and feedback, and the Princeton Department of Computer Science for providing compute resources. This work is partially supported by the Princeton School of Engineering and Applied Science.

## References

- [1] Peter Bandi, Oscar Geessink, Quirine Manson, Marcy Van Dijk, Maschenka Balkenhol, Meyke Hermsen, Babak Ehteshami Bejnordi, Byungjae Lee, Kyunghyun Paeng, Aoxiao Zhong, et al. From detection of individual metastases to classification of lymph node status at the patient level: the camelyon17 challenge. *IEEE Transactions on Medical Imaging*, 2018. [6](#)
- [2] Simon Batzner, Albert Musaelian, Lixin Sun, Mario Geiger, Jonathan P Mailoa, Mordechai Kornbluth, Nicola Molinari, Tess E Smidt, and Boris Kozinsky. E (3)-equivariant graph neural networks for data-efficient and accurate interatomic potentials. *Nature communications*, 13(1):2453, 2022. [2](#)
- [3] Gregory Benton, Marc Finzi, Pavel Izmailov, and Andrew G Wilson. Learning invariances in neural networks from training data. *Advances in neural information processing systems*, 33:17605–17616, 2020. [2](#)
- [4] Joan Bruna and Stéphane Mallat. Invariant scattering convolution networks. *IEEE transactions on pattern analysis and machine intelligence*, 35(8):1872–1886, 2013. [1](#)
- [5] Chris Burgess and Hyunjik Kim. 3d shapes dataset. <https://github.com/deepmind/3dshapes-dataset/>, 2018. [6](#)
- [6] Hamilton Y Chong, Steven J Gortler, and Todd Zickler. A perception-based color space for illumination-invariant image processing. *ACM Transactions on Graphics (TOG)*, 27(3):1–7, 2008. [2](#)
- [7] Taco Cohen and Max Welling. Group equivariant convolutional networks. In *International conference on machine learning*, pages 2990–2999. PMLR, 2016. [1, 2, 3, 10](#)
- [8] Taco Cohen, Maurice Weiler, Berkay Kicanaoglu, and Max Welling. Gauge equivariant convolutional networks and the icosahedral cnn. In *International conference on Machine learning*, pages 1321–1330. PMLR, 2019. [2](#)
- [9] Taco S Cohen, Mario Geiger, and Maurice Weiler. A general theory of equivariant cnns on homogeneous spaces. *Advances in neural information processing systems*, 32, 2019. [2](#)
- [10] Kanjar De and Marius Pedersen. Impact of colour on robustness of deep neural networks. In *Proceedings of the IEEE/CVF international conference on computer vision*, pages 21–30, 2021. [1, 2](#)
- [11] Martin Engilberge, Edo Collins, and Sabine Süsstrunk. Color representation in deep neural networks. In *2017 IEEE International Conference on Image Processing (ICIP)*, pages 2786–2790. IEEE, 2017. [1, 2](#)
- [12] Carlos Esteves, Christine Allen-Blanchette, Xiaowei Zhou, and Kostas Daniilidis. Polar transformer networks. *arXiv preprint arXiv:1709.01889*, 2017. [2](#)
- [13] Carlos Esteves, Yinsuang Xu, Christine Allen-Blanchette, and Kostas Daniilidis. Equivariant multi-view networks. In *Proceedings of the IEEE/CVF international conference on computer vision*, pages 1568–1577, 2019. [2](#)
- [14] Marc Finzi, Samuel Stanton, Pavel Izmailov, and Andrew Gordon Wilson. Generalizing convolutional neural networks for equivariance to lie groups on arbitrary continuous data. In *International Conference on Machine Learning*, pages 3165–3176. PMLR, 2020. [2](#)
- [15] Jean Gallier and Jocelyn Quaintance. *Differential geometry and lie groups*. Springer, 2020. [3](#)
- [16] Justin Gilmer, Samuel S Schoenholz, Patrick F Riley, Oriol Vinyals, and George E Dahl. Neural message passing for quantum chemistry. In *International conference on machine learning*, pages 1263–1272. PMLR, 2017. [1](#)
- [17] Samuel Greydanus, Misko Dzamba, and Jason Yosinski. Hamiltonian neural networks. *Advances in neural information processing systems*, 32, 2019. [1](#)
- [18] Sharut Gupta, Joshua Robinson, Derek Lim, Soledad Villar, and Stefanie Jegelka. Structuring representation geometry with rotationally equivariant contrastive learning. In *The Twelfth International Conference on Learning Representations*, 2023. [2](#)
- [19] Kaiming He, Xiangyu Zhang, Shaoqing Ren, and Jian Sun. Deep residual learning for image recognition. In *Proceedings of the IEEE conference on computer vision and pattern recognition*, pages 770–778, 2016. [1, 10](#)

[20] Geoffrey E Hinton, Sara Sabour, and Nicholas Frosst. Matrix capsules with em routing. In *International conference on learning representations*, 2018. 1

[21] Diederik P Kingma and Jimmy Ba. Adam: A method for stochastic optimization. *arXiv preprint arXiv:1412.6980*, 2014. 10

[22] Risi Kondor and Shubhendu Trivedi. On the generalization of equivariance and convolution in neural networks to the action of compact groups. In *International Conference on Machine Learning*, pages 2747–2755. PMLR, 2018. 2

[23] Alex Krizhevsky, Geoffrey Hinton, et al. Learning multiple layers of features from tiny images. 2009. 7

[24] Alex Krizhevsky, Ilya Sutskever, and Geoffrey E Hinton. Imagenet classification with deep convolutional neural networks. In *Advances in Neural Information Processing Systems*. Curran Associates, Inc., 2012. 1

[25] Yann LeCun, Corinna Cortes, and CJ Burges. Mnist handwritten digit database. *ATT Labs [Online]. Available: http://yann.lecun.com/exdb/mnist*, 2, 2010. 5

[26] Karel Lenc and Andrea Vedaldi. Understanding image representations by measuring their equivariance and equivalence. In *Proceedings of the IEEE conference on computer vision and pattern recognition*, pages 991–999, 2015. 1, 2

[27] Arezou Pakzad, Kumar Abhishek, and Ghassan Hamarneh. Circle: Color invariant representation learning for unbiased classification of skin lesions. In *European Conference on Computer Vision*, pages 203–219. Springer, 2022. 2

[28] Charles R Qi, Hao Su, Kaichun Mo, and Leonidas J Guibas. Pointnet: Deep learning on point sets for 3d classification and segmentation. In *Proceedings of the IEEE conference on computer vision and pattern recognition*, pages 652–660, 2017. 1

[29] Attila Lengyel Ombretta Strafforello Robert-Jan and Bruintjes Alexander Gielisse Jan van Gemert. Color equivariant convolutional networks. 2, 3, 4, 6, 10

[30] Karen Simonyan and Andrew Zisserman. Very deep convolutional networks for large-scale image recognition. *arXiv preprint arXiv:1409.1556*, 2014. 1

[31] Zikai Sun and Thierry Blu. Empowering networks with scale and rotation equivariance using a similarity convolution. In *The Eleventh International Conference on Learning Representations*, 2022. 2

[32] Nathaniel Thomas, Tess Smidt, Steven Kearnes, Lusann Yang, Li Li, Kai Kohlhoff, and Patrick Riley. Tensor field networks: Rotation-and translation-equivariant neural networks for 3d point clouds. *arXiv preprint arXiv:1802.08219*, 2018. 2

[33] Mitko Veta, Paul J Van Diest, Mehdi Jiwa, Shaimaa Al-Janabi, and Josien PW Pluim. Mitosis counting in breast cancer: Object-level interobserver agreement and comparison to an automatic method. *PloS one*, 11(8):e0161286, 2016. 1

[34] Olivia Wiles, Sven Gowal, Florian Stimberg, Sylvestre Alvise-Rebuffi, Ira Ktena, Krishnamurthy Dvijotham, and Taylan Cemgil. A fine-grained analysis on distribution shift, 2021. 10

[35] Daniel Worrall and Max Welling. Deep scale-spaces: Equivariance over scale. *Advances in Neural Information Processing Systems*, 32, 2019. 2, 4

[36] Daniel E Worrall, Stephan J Garbin, Daniyar Turmukhametov, and Gabriel J Brostow. Harmonic networks: Deep translation and rotation equivariance. In *Proceedings of the IEEE Conference on Computer Vision and Pattern Recognition*, pages 5028–5037, 2017. 2

## Appendix

### A. Datasets

#### A.1 Hue-shift MNIST

We introduce the Hue-shift MNIST dataset to evaluate the performance of our equivariant architectures in the presence of global hue shift. We show select examples from the in-distribution and out-of distribution datasets in Figures 6a and 6b.

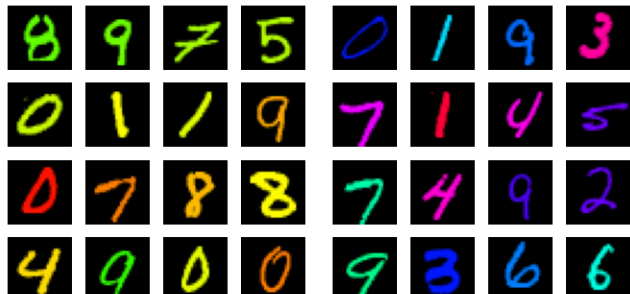
#### A.2 Hue-shift 3D Shapes

We introduce the Hue-shift 3D Shapes dataset to evaluate the performance of our equivariant architectures in the presence of local hue shift. We show select examples from the in-distribution and out-of distribution datasets in Figures 7a- 7c.

### B. Network architecture and training details

In this section we provide architectural details for our equivariant networks, and training details for each experiment.

All experiments were performed over multiple random seeds to assess the robustness of the model to initialization. Performance statistics on the Hue-shift MNIST, Hue-shift 3D Shapes, and CIFAR-10 datasets were computed over three random seeds (i.e., 1999, 2000, and 2001). Performance statistics the on Camelyon17 dataset were computed over five random seeds (i.e., 1997, 1998, 1999, 2000, and 2001).



(a) Dataset A examples

(b) Dataset B examples

Figure 6. Hue-shift MNIST dataset. (a) Examples from the training dataset and in-distribution testing dataset A are colored with a randomly selected hue between 0° and 240°. (b) Examples from out-of-distribution testing dataset B are colored with a randomly selected hue between 240° and 360°.

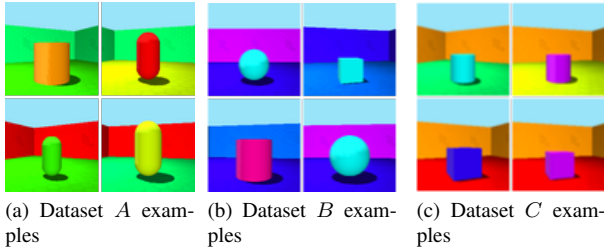


Figure 7. Hue-shift 3D Shapes dataset. (a) Examples from the training dataset and in-distribution testing dataset  $A$ . The color of the wall, the floor and the shape are randomly selected from the first half of the color space (colors 0-4). (b) Examples from the out-of-distribution testing dataset  $B$ . The color of the wall, the floor and the shape are randomly selected from the second half of the color space (colors 5-9). (c) Examples from the out-of-distribution testing dataset  $C$ . The color of the wall and the floor are randomly selected from the first half of the color space, and the color of the shape is randomly selected from the second half of the color space.

All models were trained on a shared research computing cluster. Each compute node allocates an Nvidia L40 GPU, 24 core partitions of an Intel Xeon Gold 5320 CPU, and 24GBs of DDR4 3200MHz RDIMMs.

### B.1 Hue-shift MNIST

For this task, we compare against the Z2CNN architecture proposed in Cohen and Welling [7]. Our hue-equivariant architecture has the same number of layers as Z2CNN, but with a reduced filter count to maintain a similar number of parameters at each layer. In the final layer of our hue-equivariant architecture, we perform hue group pooling to yield an hue-invariant representation.

We train our equivariant networks and the conventional architectures for 5 epochs with a batch size of 128. We optimize over a cross-entropy loss using the Adam optimizer [21] with  $\beta_1 = 0.9$ , and  $\beta_2 = 0.999$ . We use an initial learning rate of  $10^{-3}$  for the  $\mathbb{Z}^2$  network, and  $10^{-4}$  for the hue-equivariant network. We train CEConv architectures using the hyperparameters reported in [29].

### B.2 Hue-shift 3D Shapes: Local hue equivariance

For this task we compare against the ResNet18 architecture proposed in [19], and the Z2CNN and ResNet44 architectures proposed in [7]. Our hue-equivariant architectures are designed with the same network structure as the baselines, but with a reduced filter count to maintain a similar number of parameters at each layer. In the final layer of our hue-equivariant architectures, we perform hue group pooling to yield an hue-invariant representation.

Following [34], we train the ResNet architectures for 100k iterations with a batch size of 128. We optimize over a

cross-entropy loss using SGD with a learning rate of  $10^{-2}$ . Images are down-sampled by a factor of 2 to train the CNN architectures. CNN architectures are trained as described in Section B.1.

### B.3 CIFAR-10: Color shift in the wild

For this task, we compare against the ResNet44 architecture proposed in [7]. Our hue-, saturation- and hue-saturation-equivariant architectures have the same number of layers as ResNet44, but with a reduced filter count to maintain a similar number of parameters at each layer. In the final layer of our networks, we perform group pooling to yield group invariant representation.

We train our equivariant networks and the conventional architectures for 300 epochs, and a batch size of 128. We optimize over a cross-entropy loss using SGD with an initial learning rate of  $10^{-1}$  and a cosine-annealing scheduler. We train CEConv architectures using the hyperparameters reported in [29].

### B.4 Camelyon17: Saturation shift in the wild

For this task, we compare against the ResNet50 architecture [19]. Our hue- and saturation-equivariant architectures have the same number of layers as ResNet50, but with a reduced filter count to maintain a similar number of parameters at each layer. In the final layer of our hue- and saturation-equivariant architectures, we perform a group pooling to yield group invariant representation.

We train our equivariant networks and the conventional architectures for 10k iterations with a batch size of 32. We optimize over a cross-entropy loss using the Adam optimizer [21] with an initial learning rate of  $10^{-2}$ ,  $\beta_1 = 0.9$ , and  $\beta_2 = 0.999$ . We train CEConv architectures using the hyperparameters reported in [29].

### C. Hue and saturation group action

In this section we prove the proposed hue group action and saturation group action satisfy the axioms for a group action. By definition of a group action,  $\varphi_h$  is a group action if it satisfies the following properties:

1. For all  $g, h \in G$  and all  $x \in X$

$$\varphi(g, \varphi(h, x)) = \varphi(gh, x) \quad (21)$$

2. For all  $x \in X$

$$\varphi(1, x) = x \quad (22)$$

where  $1 \in G$  is the identity element of  $G$ .

In the remainder of this section we refer to equation 21 as ‘property one’ and equation 22 as ‘property two’.

## C.1 Hue group action

Here we show that the proposed hue group action is indeed a group action. The proposed hue group action on the input space is defined:

$$\varphi_h(h_i, x) = ((x_h + h_i) \pmod{255}, x_s, x_l), \quad (23)$$

in equation 7 of the main text.

First we show the proposed hue group action  $\varphi_h$  satisfies property one. For any hue shifts  $h_i$  and  $h_j$ , we have

$$\varphi_h(h_i, \varphi_h(h_j, x)) = \varphi_h(h_i, ((x_h + h_j) \pmod{255}, x_s, x_l)) \quad (24)$$

$$= (((x_h + h_j) \pmod{255} + h_i) \pmod{255}, x_s, x_l) \quad (25)$$

$$= (((x_h + (h_j + h_i)) \pmod{255}, x_s, x_l)) \quad (26)$$

$$= \varphi_h((h_j + h_i), x), \quad (27)$$

which shows that  $\varphi_h$  satisfies the property one. Now we show  $\varphi_h$  satisfies property two. We have the identity element hue transformation  $h_0 = 0$ , and

$$\varphi_h(h_0, x) = ((x_h + h_0) \pmod{255}, x_s, x_l) \quad (28)$$

$$= (x_h, x_s, x_l) = x, \quad (29)$$

which shows  $\varphi_h$  satisfies property two. Having shown that  $\varphi_h$  satisfies all properties of a group action, we have that  $\varphi_h$  is, in fact, a group action.

## C.2 Saturation group action

Here we show the proposed saturation group action is a group action. The proposed saturation group action is defined:

$$\varphi_s(s_i, x) = (x_h, \min(x_s + s_i, 255), x_l), \quad (30)$$

in equation 9 of the main text. First we show the proposed saturation group action  $\varphi_s$  satisfies property one. For any saturation shifts  $s_i$  and  $s_j$ , we have

$$\varphi_s(s_i, \varphi_s(s_j, x)) = \varphi_s(s_i, (x_h, \min(x_s + s_j, 255), x_l)) \quad (31)$$

$$= (x_h, \min(\min(x_s + s_j, 255) + s_i, 255), x_l) \quad (32)$$

$$= (x_h, \min(x_s + (s_j + s_i), 255), x_l) \quad (33)$$

$$= \varphi_s((s_j + s_i), x), \quad (34)$$

which shows  $\varphi_s$  satisfies property one. Now we show  $\varphi_s$  satisfies property two. We have the identity element saturation transformation  $s_0 = 0$ , and

$$\varphi_s(s_0, x) = (x_h, \min(x_s + s_0, 255), x_l) \quad (35)$$

$$= (x_h, x_s, x_l) = x, \quad (36)$$

which shows  $\varphi_s$  satisfies property two. Having shown that  $\varphi_s$  satisfies all properties of a group action, we have that  $\varphi_s$  is, in fact, a group action.